Ca-doped zirconia mesoporous coatings for biomedical applications: A physicochemical and biological investigation

Francesca Tana[a,b], Elvira De Giglio[c], Stefania Cometa[d], Agnese D'Agostino[b], Andrea Serafini[a], Fabio Variola[e], Nina Bono[b], Roberto Chiesa[a,b,*], Luigi De Nardo[a,b]

[a] National Interuniversity Consortium of Materials Science and Technology (INSTM), Local Unit Politecnico di Milano, Via Giusti 9, 50121, Firenze, Italy
[b] Department of Chemistry, Materials and Chemical Engineering "G. Natta", Politecnico di Milano, Milano, Italy
[c] Department of Chemistry, Università di Bari Aldo Moro, Bari, Italy
[d] Jaber Innovation srl, Via Calcutta 8, 00100, Roma, Italy
[e] University of Ottawa, Department of Mechanical Engineering, Ottawa, Ontario, Canada

ARTICLE INFO

Keywords:
Surface nanotopography
Self-assembly
Mesoporous zirconia coating
Calcium doped-zirconia
Cell growth

ABSTRACT

In this work, the effects of surface chemistry and nano-topography of un-doped and Ca-doped zirconia coatings were investigated. The study aimed at providing new insight on how to improve the interfacial properties and biocompatibility of metallic and ceramic biomedical implants for hard tissue applications through the surface modification treatments. To this end, pure and Ca-doped zirconia mesoporous coatings were prepared by wet synthesis and structure self-assembly. The physicochemical properties of mesoporous surfaces were investigated by TEM and XRD. In addition, contact angle and XPS unveiled the wettability and surface chemistry of zirconia surfaces. Our findings highlight the role of Ca in increasing stability of the mesoporous structure at high calcination temperature, applied to remove the templating agent. In vitro assays focused on the proliferation of Saos-2 human osteoblastic cells on the meso-structured zirconia coatings, which resulted to be enhanced on Ca-doped surfaces.

1. Introduction

Since the first successful discovery by Mobil group of MCM-41 (Mobil Composition of Matter) and M41S silica molecular sieves [1], numerous efforts have been focused on the fabrication of non-silicate-based materials with mesoporous structures (i.e. pore size of 2–50 nm in diameter). Recently, inorganic mesoporous materials, including metal oxides (e.g. TiO_2, CeO_2, ZrO_2), have attracted widespread interest as a fundamental and technological challenge, offering promising potential for electronic, magnetic, optical applications, catalyst and sensor design [2,3], as well as in biomedical field [4–6].

In biomedical applications, the main challenge associated with implantable materials is their biocompatibility and tissue integration: in the case of orthopedic, spinal, and dental applications, the success of the implant material is due to its ability to integrate into the surrounding bone. In this context, metals and alloys such as titanium, titanium alloys, cobalt chromium alloys (Co-Ni-Cr, Co-Cr-Mo), and stainless steels have been widely employed (e.g. for dental, orthopedic and cardiovascular implants, surgical instruments, prostheses and orthodontic devices) by capitalizing on their excellent corrosion resistance, biocompatibility, chemical and mechanical properties, as well as on their good processability into complex geometries [7]. In the case of dental implants, titanium has been for decades the metal of choice. However, a main limitation of titanium used for dental implants is related to its metallic appearance arising from the thin mucosa in anterior dental implants, which thus negatively affects its esthetics [7]. In addition, titanium and titanium alloys are susceptible to fretting corrosion, and the protective titanium oxide can be damaged, resulting in a release of metal ions in the surrounding tissues. Such degradation products may induce hypersensitivity in susceptible patients, increasing the possibility of implant failure [8].

Because of these limitations, research of new suitable material for implant technologies is constantly developing. In this context, bulk zirconia (ZrO_2) components have been widely used in dentistry as a valid alternative to metals due to their mechanical reliability and aesthetic similarity with natural teeth. Among the components available in the market, dental crowns, fixtures and abutments have been rapidly diffusing in dentistry. Of note, the chemical and mechanical properties which ensure suitability of zirconia in biomedical applications are strictly connected to its allotropic structures: monoclinic, tetragonal

and cubic [9]. Since the transformation from the metastable tetragonal phase to the monoclinic phase decrease surface hardness and mechanical strength, the stability of tetragonal phase is crucial for the in vivo success of zirconia implants. To achieve a proper structural stability and mechanical safety, the crystalline tetragonal structure can be stabilized by incorporating yttrium, cerium, calcium and magnesium oxides [10,11].

A large body of literature has demonstrated the importance of the physicochemical and topographical surface properties (i.e. roughness and nanoscale morphology) in the interactions between the biological environment and synthetic substrates [12,13].

Based on this evidence, it is now clear that the rationale design of the surface properties is key to direct fundamental cellular and molecular events at the implant–host tissue interface [14], towards an improved biological outcome (e.g. the osteointegration) of implanted devices [14–17].

From a biological point of view, zirconia naturally promotes cell proliferation and differentiation towards the osteogenic pathways [18]. It also showed good osteointegrative properties, making it an option for direct bone fixation of implants [18]. Notably, zirconium oxide surface modifications were reported to improve the initial bone healing and to increase the fixation of dental implants [19–21]. In particular, several surface treatments, aimed at modulating both morphology (i.e., porosity and roughness) and chemistry, have been proposed and applied to clinical practices [21,22]. Among these, acid etching, alumina sandblasting, or microgrooves addition on zirconia implants surface [19] have been proposed, while chemical surface modifications have been based on bioactive glass [20] or calcium phosphate coatings [21] on bulk zirconia, showing improved bioactivity. Among the surface modification approaches developed to date, those capable of engendering mesoporous structures have rapidly emerged as a valid alternative to endow materials (silica [23], titanium [24], polymers, carbon [5] and silicon [6]) with new bioactive abilities. Porous structures were in fact reported to support and control cell adhesion, growth and proliferation on different materials, proving that cell fate is influenced even by pores as small as a few nanometers (~5 nm) in diameter [4]. Moreover, the adsorption, diffusion and physical entrapment of proteins into the pore network is expected to further enhance cell attachment and growth [25,26].

In this context, despite the advances in the investigation of zirconia components for biomedical applications [27], a better comprehension of the structure–function relationship of mesoporous zirconia coatings still needs to be fully addressed. In particular, although the synthesis of zirconium oxide mesoporous phases with hexagonal [28], or cubic pore structure [29,30] via metal precursors and sacrificial template agents has been already investigated, none of these structures were investigated with regards to cell compatibility, adhesion and growth.

Distinctively from previous studies, we investigated a new strategy aimed at enhancing cell adhesion and proliferation on medically relevant materials based on the deposition of a overlying mesoporous zirconia coating by sol–gel. The combination of a sol–gel process and self-assembly techniques has in fact proven to be one of the most effective methods for bottom-up synthesis of complex tailor-made nanostructured inorganic materials [31,32]. The addition of both soft (e.g. block copolymers, ionic liquids, biopolymers) and hard templates [28,33] to the precursor mixture and their subsequent removal, allows obtaining a final porous inorganic network for direct cuing to adhering cells.

By capitalizing on the addition of a soft copolymer in the precursor sol–gel mixture, pure and Ca-doped mesoporous zirconia surfaces were created for the first time. Calcium was added to the precursor mixture both to stabilize zirconia phase evolution [9] and to improve the thermal resistance of the porous zirconia network. Of note, calcium is a component known to positively affect relevant biological functions such as protein binding and biomineralization [34,35,36]. The resulting Ca-doped zirconia was successively deposited as thin mesoporous film by spin coating on cover glasses, and cell cultures with Sao2 cells were carried out.

2. Materials and methods

2.1. Chemical reagents

Zirconium (IV) tetrachloride ($ZrCl_4$) was supplied by ABCR (Germany). Ethanol (EtOH), Pluronic F127 (poly(ethylene oxide)$_{106}$–poly(propylene oxide)$_{70}$–poly(ethylene oxide)$_{106}$, PEO_{106}–PPO_{70}–PEO_{106}) block copolymer and $Ca(NO_3)_2$ hydrate, were purchased from Sigma Aldrich (Sigma–Aldrich S.r.l., Italy). Cover glasses (diameter 15 mm) were supplied by BioOptica (Italy).

All chemicals were used as received without any further purification. Millipore water was used when aqueous solutions were employed.

2.1.1. Synthesis of zirconia mesoporous coatings

The precursor solution was prepared by mixing two solutions, the first one containing metal chloride $ZrCl_4$ 0.346 g ($1.5 * 10^{-3}$ mol) in 2 mL 90% EtOH and the second one containing a solution of commercially available ABA block copolymer, Pluronic F127, ($EO_{106}PO_{70}EO_{106}$) 1.7 g in 2 mL 90% EtOH. The final mixture resulted in acidic solutions, which prevented precipitation [28]. Mixed Ca- doped zirconia solutions were obtained in the same way, i.e. by adding 11% mol ($1.6 * 10^{-4}$ mol) and 25% mol. ($3.7 * 10^{-4}$ mol) of $Ca(NO_3)_2$ precursor to the starting zirconium chloride solution in ethanol. The resulting samples were labeled Z_T, Ca_T, and $Ca25_T$, where Z was used to identify the pure zirconia coatings while Ca and Ca25 were associated with 11% and 25% Ca-doped zirconia samples, respectively. The footer $_T$ stands for the applied calcination temperature (400–500–600 °C). Ex- perimental parameters are summarized in Table 1.

Films were prepared by spin-coating glass substrates, according to a profile which consisted of a ramp of 10 s until 200 rpm subsequently followed by 15 s at 500 rpm. The subsequent aging and consolidation steps are displayed in Fig. 1. Immediately after the first drying process in oven at 100 °C for 12 h, films were stored for 1 day at 37–40 °C in a closed vessel, with a relative humidity of 40%. A thermal treatment was then performed at 400, 500 or 600 °C in air for 3 h to remove the template and making the crystalline phase evolution visible. Non-templated pure zirconia surfaces were prepared in the same way and used as controls: the $ZrCl_4$ precursor solution with no addition of template agent was deposited on cover glass.

2.1.2. Physicochemical characterization

Zirconia coatings were analyzed by transmission electron microscopy (TEM, Philips CM 200 field emission gun) to close in on the pore size, the morphology and the crystallinity. Bright-field TEM and selected area electron diffraction (SAED) were carried out by using an accelerating voltage of 200 kV. For TEM observation, samples were prepared as follows: cover glass substrate was first spin coated by a polylactic acid (PLA) solution in chloroform and then covered by the prepared precursor solutions. After coating consolidation (12 h at 100 °C), the sacrificial PLA coating was removed in chloroform and slices of the mesoporous structure were recovered by immersing TEM grids in the solution, followed by calcination at different temperatures.

The evolution of crystalline phases on mesoporous samples induced

Table 1
Composition details and code for pure zirconia and Ca-doped coated samples.

Sample code	Composition (mol)		Calcination temperature (°C)		
	$ZrCl_4$	$Ca(NO_3)_2$	400	500	600
Z_T	$1.5 * 10^{-3}$	/	Z_{400}	Z_{500}	Z_{600}
Ca_T	$1.5 * 10^{-3}$	$1.6 * 10^{-4}$	Ca_{400}	Ca_{500}	Ca_{600}
$Ca25_T$	$1.5 * 10^{-3}$	$3.7 * 10^{-4}$	$Ca25_{400}$	$Ca25_{500}$	$Ca25_{600}$

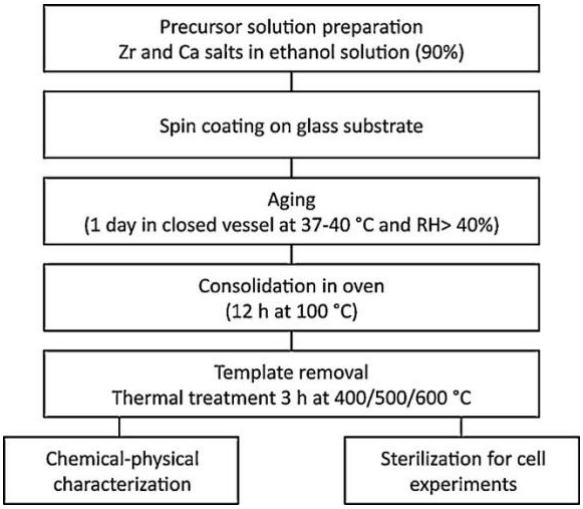

Fig. 1. Protocol for the preparation of coatings.

by thermal treatment was tracked by X-ray diffractometry (XRD, Philips PW 1830) equipped with a Bragg Brentano diffractometer and Cu-Kα1 radiation (wavelength: 0.154056 nm). The X-ray diffraction patterns were collected at room temperature in 10-70° 2θ range, setting 0.5 s as scanning time per step and a scan step size of 0.02 degrees. Crystalline phases were assigned on the base of Panalytical XPert Data and JPCDS database.

Static contact angle measurements were performed on calcined samples by depositing distilled water drops of about 5 μL. Measurements were acquired through goniometer instrumental set-up using an image elaboration software (Drop Shape Analysis). Measurements were repeated in duplicate, five time each sample.

X-ray photoelectron spectroscopy (XPS) analysis was performed to gain information on the surface chemical composition of the mesoporous coatings. The analysis was carried out by a scanning microprobe PHI 5000 VersaProbe II (Physical Electronics, Chanhassen, MN), equipped with a monochromatized AlKα X-ray radiation source. The samples were analyzed in HP mode (scanned size ~ 1400 × 200 μm), with an X-ray take-off angle of 45°. For each sample, survey scans and high-resolution spectra were recorded in Fixed Analyzer Transmission (FAT) mode (pass energy 117.4 eV and 29.35 eV, respectively). Data analysis was performed using the MultiPak software package (version 9.6.1.7). The normalization of the peak area and comparison of data from different elements was enabled by correction with empirically derived sensitivity factors according to MultiPak library. Charge referencing was performed by setting the lower binding energy C1s photopeak (i.e., C1s hydrocarbon peak) at 284.8 eV.

2.2. Cells culture medium and biological reagents

1X McCoy cell culture medium, Fetal Bovine Serum (FBS), Glutamine (Glut), Penicillin-Streptomicin (PS), Sodium Pyruvate (Pyr), resazurin, gluteraldehyde 70% and Phosphate Buffer Saline solution (PBS) (P8537) were purchased from Sigma (Italy). All chemicals were

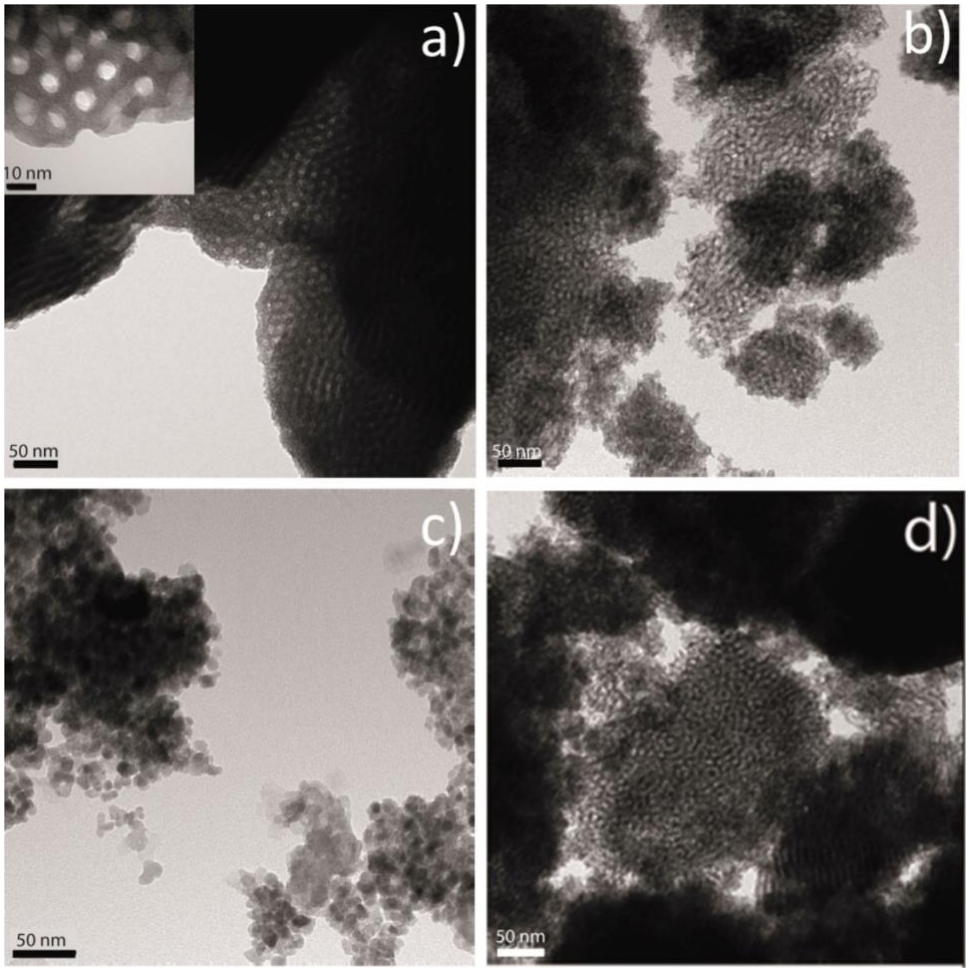

Fig. 2. Representative TEM micrographs of a) pure zirconia and b) Ca25 zirconia mesoporous samples calcined at 400 °C, c) pure zirconia and d) Ca25 zirconia calcined at 600 °C.

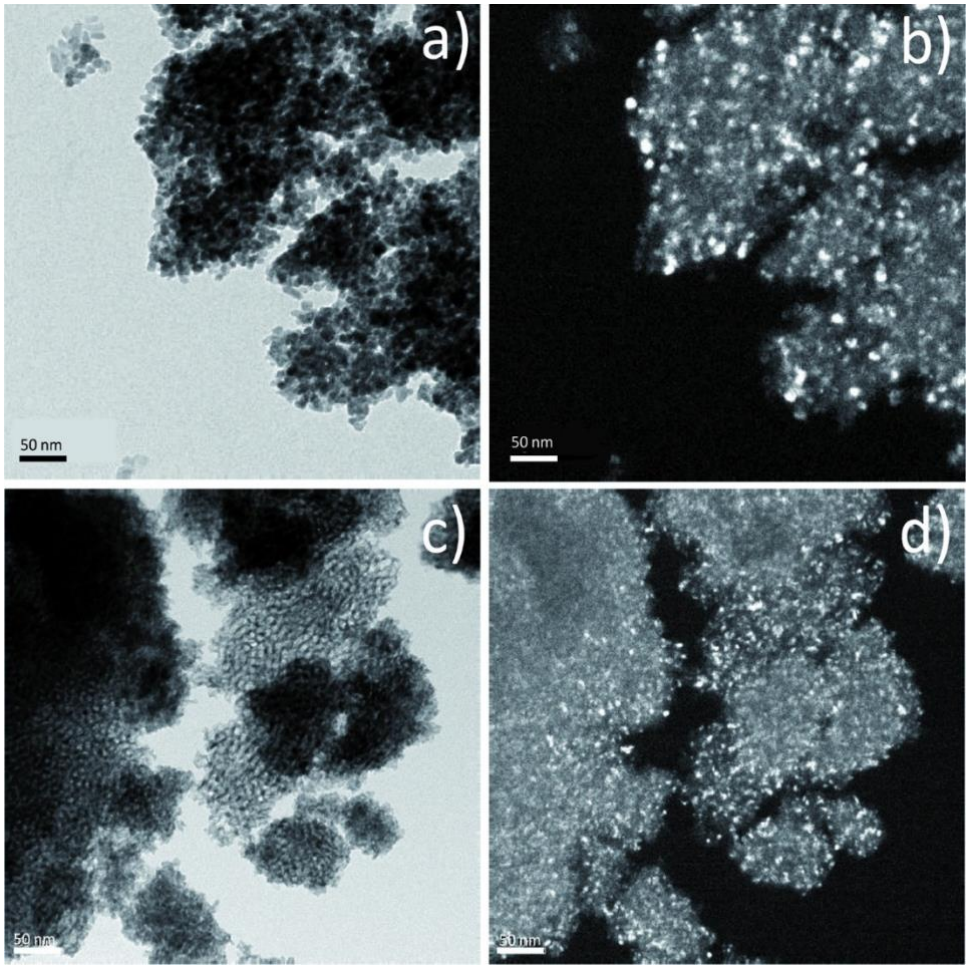

Fig. 3. Representative TEM images of a) and b) Z samples calcined at 600 °C, and c), d) Ca25 zirconia calcined at 600 °C, bright and dark-field, respectively.

used under biological hood in sterile conditions.

2.2.1. Cells medium preparation

Biological assays were carried out with SAOS-2 human osteoblast-like cell line. Cells were grown in a SAOS-2 medium composed as follow (reported percentage and concentration are referred to the final volume): 500 mL of 1X McCoy cell culture medium (with $NaHCO_3$, glutamine free), 90 mL of previously filtered FBS (15%), 6.0 mL of glutamine (2 mM), 6.0 mL of penicillin-streptomicin (1%), and 6.0 mL of sodium pyruvate (1 mM). After seeding, cells were maintained at 37 °C in a humidified atmosphere containing 5% CO_2. The culture medium was replaced every three days.

2.2.2. Cell seeding and culture

Before seeding, samples (glass controls and porous/non porous zirconia coatings) were disinfected by ethanol immersion (30 min) and sterilized by UVC light under biological hood (15 min each side). Treated cover glasses (15 mm diameter) were then inserted horizontally on the bottom of 24-well culture flasks.

The cells were seeded at a density of $10^4\,cm^{-2}$ ($1.9*10^4$ cells per well), adding a volume of 500 µL of culture medium, and cultured up to 14 days. A triplicate for each sample for each time point was tested during cytocompatibility tests.

2.3. In vitro assays

2.3.1. Cell viability

At given time point (i.e. 1, 3, 7, 10, and 14 days) resazurin microtiter assay (Alamar blue test) was performed on cultured samples. To this end, culture medium was removed from each well and replaced with the same volume of culture medium containing 1× resazurin dye (500 µL/well). Samples were incubated at 37 °C (5% CO_2, 100% humidity) for 4 h, and then the fluorescence of the medium was read with a GENios Plus reader (Tecan, Segrate, Italy) (λex =540 nm; λem =595 nm). For each sample, measurements were carried out in triplicate. Data have been expressed as the mean ± standard deviation and compared statistically by Student's t-test. (p-values of <0.05 and <0.01 were considered statistically significant.)

2.3.2. Cell morphology

Two samples per category were removed after 1, 3, 7 and 14 days of incubation in culture media, rinsed twice with PBS to remove non-adherent cells and finally fixed with 1.5% of glutaraldehyde 70% in PBS for 2 h. Successively, samples were immersed in water/ethanol solution (with increasing ethanol content, from 10% to pure ethanol), and finally sputtered with gold palladium for Scanning Electron Microscopy (SEM, StereoScan 360, Cambridge Instruments) observation.

3. Results

3.1. Morphological and structural characterization

Fig. 2 shows a representative TEM image of pristine zirconia and Ca25 zirconia mesoporous samples, calcined at 400 °C (a and b), and 600 °C (c and d), respectively. A mesoporous structure, with pores in the 5-10 nm diameter range, were observed in Z_{400} and $Ca25_{400}$

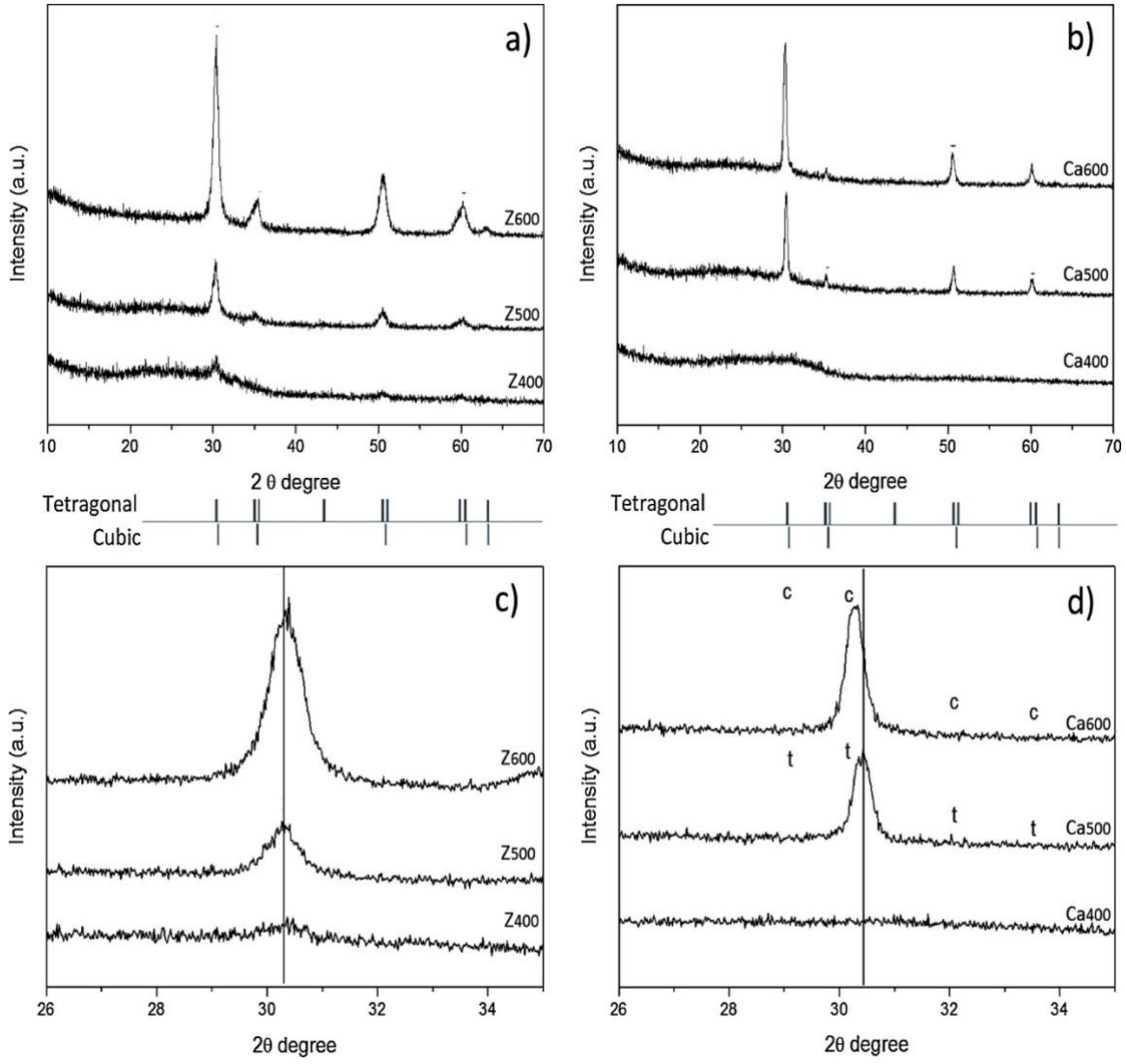

Fig. 4. Representative XRD spectra of a) pure zirconia and b) Ca-doped samples calcined at 400, 500 and 600 °C (Z_{400}, Z_{500}, Z_{600} and Ca_{400}, Ca_{500}, Ca_{600},) and the respective zoom c) and d) showing the peak shift in Ca_{600} sample.

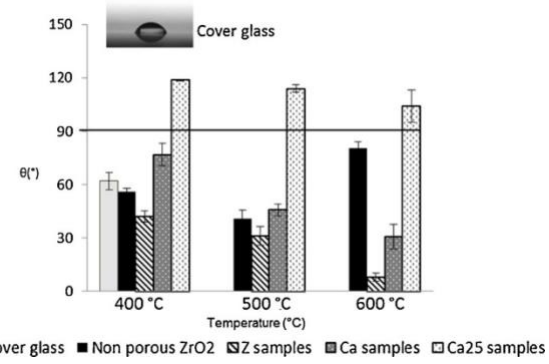

Fig. 5. Static contact angle measurements on pure and Ca-doped samples calcined at different temperatures (400–500–600 °C). The line sets the limit of 90° for hydrophilic (< 90°) and hydrophobic (> 90°) surfaces.

samples (Fig. 2a and b). Of note, a mesoporous framework was also observed in $Ca25_{600}$ sample (Fig. 2d), while small crystals formed in pure zirconia samples calcined at 600 °C (Fig. 2c).

The *in situ* structural evolution of nanocrystals was further analyzed by comparing bright and dark-field TEM observations (Fig. 3). The existence of several nanocrystallites was shown both for Z and Ca25 samples, with the latter being smaller than the corresponding Z samples both in 400 (data not shown) and 600 °C calcined samples, as indicated by the white crystals in Fig. 3b and d.

Fig. 4a and b summarize the results of wide angle XRD analysis for ZrO_2 coatings at different calcination temperature (400–600 °C). For samples annealed at 400 °C (Z400, Ca400), broad diffraction peaks are evident, indicating that the oxide structure is only partially crystallized. By increasing the calcination temperature to 500 °C, well-defined peaks associated with the tetragonal/cubic phase appear in analyzed samples.

3.2. Surface characterization

Surface wettability was assessed by static contact angle, to investigate the effects of processing temperatures on the structure and the coating composition. The contact angle results are summarized in Fig. 5.

The presence of calcium in deposited coatings was confirmed by XPS analysis on mesoporous coatings. Zr-based systems showed a main XPS region relevant to Zr3d, having well resolved spin-orbit components ($Zr3d_{3/2}$ and $Zr3d_{5/2}$, at 182.0 ± 0.2 eV and 184.4 ± 0.2 eV, respectively, with a typical $\Delta_{BE} = 2.4$ eV), and a secondary signal of Zr3p. This latter falls at BEs overlapping those of the Ca2p signal,

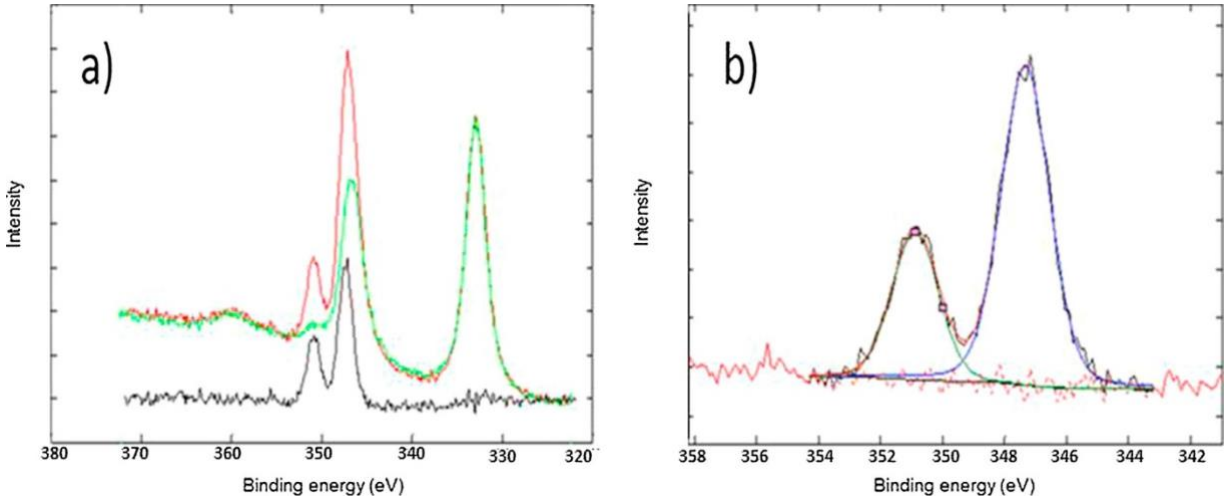

Fig. 6. a) Zr3p spectrum difference (black line) of $Ca25_{400}$ (red line) and Z_{400} (green line), b) Ca2p signal resulting from the spectrum difference of panel a). (For interpretation of the references to colour in this figure legend, the reader is referred to the web version of this article).

Table 2
Surface elemental composition (atomic percentages, At%) determined by XPS on pure zirconia and Ca-doped coated samples.

Sample code	C1s	O1s	Zr3d	Na1s	Si2p	P2p	Ca2p	Ca/Zr *100
Z_{400}	29.1	45.9	16.5	4.8	3.7	-	-	
Ca_{400}	43.7	38.4	12.4	0.5	4.2	-	0.8	6.5%
$Ca25_{400}$	36.0	43.3	10.6	0.4	3.1	2.6	4.0	37.7%
Z_{600}	16.0	53.5	16.2	6.0	8.3	-	-	
Ca_{600}	16.6	56.1	22.7	1.4	1.5	0.6	1.1	4.8%
$Ca25_{600}$	13.9	56.9	22.2	1.1	3.8	-	2.1	9.5%

therefore, a spectrum difference between Zr3p signals of pure zirconia and Ca-doped zirconia was performed to evaluate calcium contribution (see Fig. 6a). The spectrum difference result (see Fig. 6b) was a typical doublet ascribable to Ca2p signal (i.e., $Ca2p_{3/2}$ and $Ca2p_{1/2}$, at 347.0 ± 0.2 eV and 350.5 ± 0.2 eV, respectively). On the other hand, considering the Ca2s signal (439.2 ± 0.2 eV), it was also involved in an overlapping with Zr3s signal (432.8 ± 0.2 eV) (data not shown).

However, by the curve fitting of the Ca2s signal, both calcium and zirconium contributions could be distinguished and this further confirmed the atomic percentages and the Ca/Zr ratios obtained by the above reported spectrum difference procedure. Surface atomic percentages relevant to pure and Ca-doped samples calcined at 400 and 600 °C are reported in Table 2.

The XPS atomic percentages confirmed a higher presence of residues of partially combusted organic byproducts inside the pores at lower calcination temperatures (see the higher C1s percentage in the 400 °C calcined systems with respect to the 600 °C ones). Moreover, Ca/Zr corrected area ratios, reported in the last column of Table 2, evidenced a variable calcium surface amount: $Ca25_{400} > Ca25_{600} > Ca_{400} > Ca_{600}$.

3.3. Material-cell interaction: cytocompatibility tests

Osteoblastic SAOS-2 cells were cultured for up to 14 days on pure and Ca-doped substrates calcined at 400 °C. These samples were chosen as the most representative, since the presence of porous network was confirmed by TEM. Fig. 7a reports cells viability results obtained on Z_{400}, Ca_{400} and $Ca25_{400}$ surfaces.

An increased viability during the observed 14 days confirmed that all samples support cell adhesion and proliferation. At day 1, all tested samples displayed similar values of cell viability. However, at day 3, an evident increase in cell viability was observed, with observable differences for Ca-containing samples (i.e. Ca_{400} and $Ca25_{400}$) in comparison with the non-porous substrate ($p < 0.05$ and $p < 0.01$, respectively). Cell viability increasingly grew with time and significant differences were found for all tested samples at day 7 in comparison with non-porous surfaces ($p < 0.05$, $p < 0.01$ and $p < 0.05$ for Z_{400}, Ca_{400}, and $Ca25_{400}$, respectively). Fig. 7b shows that adhering cells assumed a well-spread and elongated morphology on all surfaces.

4. Discussion

4.1. The role of Ca in mesoporous zirconia morphological and crystalline phase stabilization

The synthesis and characterization of inorganic mesoporous structures of pure and Ca-doped zirconium oxide were carried out by employing zirconium tetrachloride as a non-expensive inorganic precursor to engender mesoporous frameworks via industrially available ABA, hazard-free, and easy to remove templates. The effects of an increase in the calcination temperature were studied by focusing on the zirconia phase evolution and the induced morphological changes in mesoporous structures.

As previously reported, the introduction of an amphiphilic block copolymer (as Pluronic ABA template) promotes the formation of large pores with a diameter in the 5-20 nm range [32]. An aging procedure under controlled humidity (40%, at a fixed temperature of 40 °C) was necessary to enable the growing structure to self-organize [30,37]. Nonetheless, the potential disorder in pore distribution was not considered as a limitation for the final application and furthermore, random nano-topography was reported to have a positive effect on the cellular adhesion and differentiation in comparison with highly ordered nano-topography [38]. In addition to morphology, the pore size was reported to have a relevant role in dictating interactions with biological environments [5].

As the calcination temperature was increased from 400 to 600 °C, the mesoporous structure of pure ZrO_2 collapsed. This was attributed to the extended growth of crystallites and diffuse sintering that lead to a rapid pore coarsening [32,37,39] a finding that was further supported by XRD measurements. Notably, this phenomenon was reduced in Ca-doped structures (Fig. 2d) and the high stability of $CaO-ZrO_2$ solid-solution at the higher temperature could be crucially attributed to the doping effect of Ca^{2+} [40]. The introduction of doping ions during the formation of ZrO_2 network is believed to slow down the growth rate of nano-crystallites [37].

The induced crystallization of the amorphous component in the

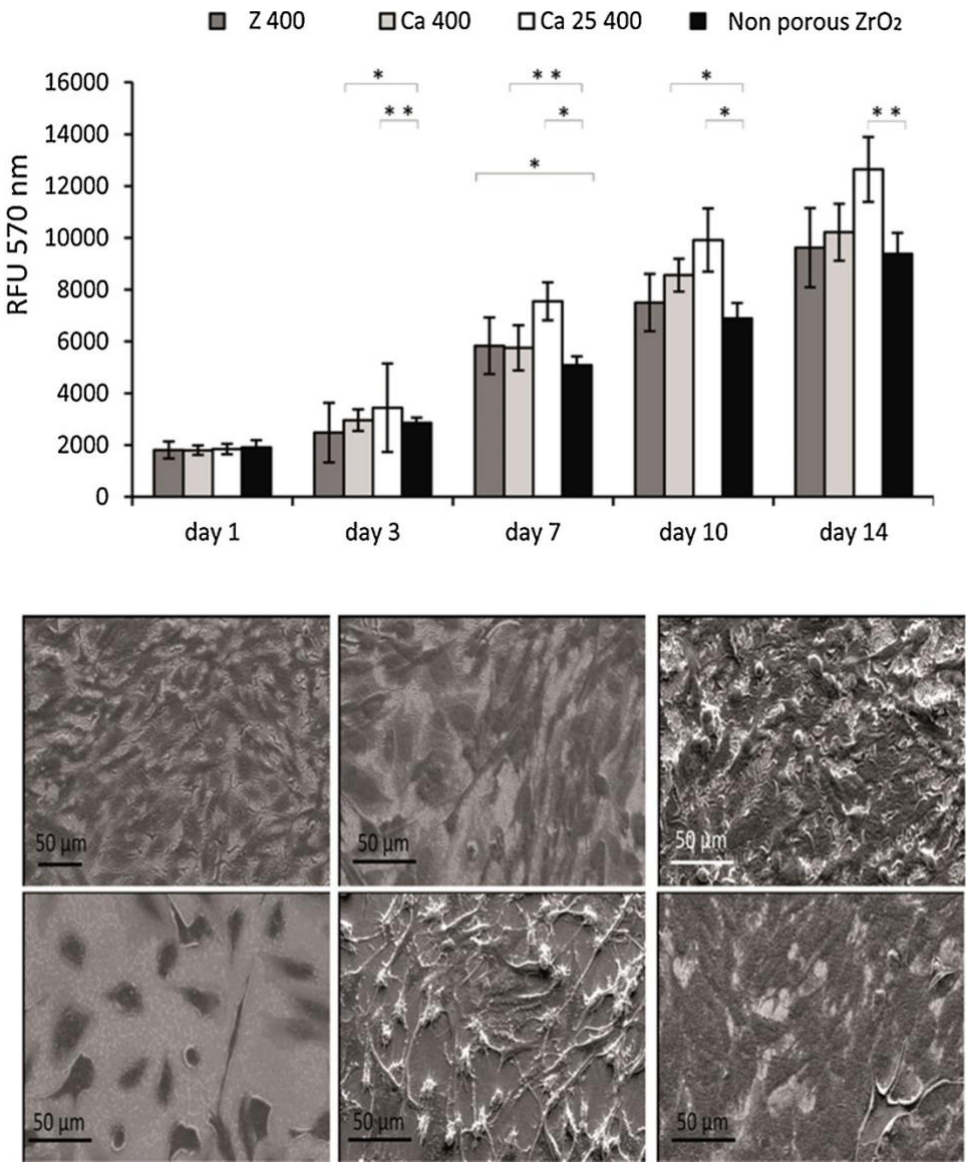

Fig. 7. a) Cell viability results performed by Alamar blue test with osteoblasts-like SAOS-2 cells cultured for 14 days on non-porous ZrO_2 surfaces, pure and Ca-doped ZrO_2 porous coatings calcined at 400 °C; b) Z_{400} (top) and $Ca25_{400}$ cultured samples (down) at day 3, 7 and 14. (For interpretation of the references to colour in this figure legend, the reader is referred to the web version of this article).

zirconia network is expected to lead to a concomitant phase transformation. It is now well known that zirconia naturally occurs in different crystalline phases depending on the environmental conditions [9]. The monoclinic phase is the thermodynamically stable phase of zirconia from room temperature to 1170 °C. Nonetheless, the addition of stabilizing agents (e.g. divalent and trivalent cationic specie such as Mg^{2+}, Ca^{2+}, Cr^{3+}, and Y^{3+}) [9,11,30], or some critical dimensions of the crystal (in the range of approximately 30 nm), allow the metastable tetragonal phase to grow [41].

These observations support TEM results, validating the evolution and the stability of the porous structure, which thus undergoes both morphological and crystalline structure modifications in response to increasing temperatures. The transition from amorphous to tetragonal zirconia at approximately 480 °C was previously reported [42]. The incorporation of low-valent cations by structure doping further stabilizes the more symmetric tetragonal and cubic phase due to the oxygen vacancies introduced in the lattice [43]. The absence of diffraction lines corresponding to CaO crystallites in Ca-doped samples suggests that homogeneous CaO-ZrO_2 solid solution formed [44]. The observed peak shift in Ca-doped samples Ca_{600} revealed lattice strain due to the substitutional or interstitial replacement of Ca^{2+} by Zr^{4+} ions. The variation of lattice parameters was probably caused by differences in ionic radius between the two ions, as previously reported for other metal oxides [45]. Notably, in the observed range of temperature, no phase transformation from tetragonal to monoclinic was observed in pure zirconia samples as in other reported synthesis [37].

4.2. Effects of mesoporous structure on surface properties

Contact angles measurements and XPS analysis were carried out to understand the effects of mesoporous structure on surface properties.

Generally, the slight decrease of the contact angle values is observed with rising annealing temperature, because of increasing in crystallinity. However non-porous zirconia sample at 600 °C shows an opposite trend that could be attributed to the de-hydroxylation of the surface or caused by air trapped underneath the water droplets [46]. The successful introduction of mesoporosity decreased the water contact angle due to well-known surface roughness effect and resulted in hydrophilic coatings [47].

On the other hand, a large increase of the contact angle with

increasing Ca content was observed. This could be explained by considering the presence of residues of partially combusted organic byproducts inside the pore at lower calcination temperatures. The presence of these organic byproducts may in fact increase the overall hydrophobicity of the surface and it was especially evident when comparing pure zirconia to Ca25 samples. As expected, the amount of detected calcium is lower in Ca samples in comparison with the higher loaded ones, Ca25. This was further confirmed by XPS measurements. Nevertheless, with the exception of $Ca25_{400}$, all the analyzed coatings revealed a minor calcium content in comparison with the nominal amount in the solution.

However, further XPS analysis at other calcination temperature are necessary to support the contact angle results and to better understand the wettability of this kind of mesoporous coatings.

4.3. Influence of mesoporous structure on cell-surface interaction

The very first assessment of a biomaterial in vitro relies on the evaluation of the overall biocompatibility and the identification of the possible cell-biomaterial interactions. These are essential aspects for scaffold materials to properly support cell growth in vitro and eventually tissue integration *in vivo*.

In this study, we evaluated and compared the effect of different substrates, namely non-porous, pure and Ca-doped ZrO_2 porous coatings, on cell behavior in vitro. Our preliminary in vitro findings (Fig. 7) suggested a possible active role on cell proliferation exerted by the mesoporous surfaces when compared to the non-porous counterparts. Among the mesoporous coating, $Ca25_{400}$-doped samples reported the highest proliferation rate, probably because of the high amount of Ca in such materials.

This is not surprisingly since the addition of calcium additives in materials for biomedical applications has been extensively reported in literature [35], demonstrating that higher levels of mineralization were observed with increasing amounts of CaO.

However, further investigations are needed to strengthen our findings and to shed light on how Ca-doped mesoporous coatings influence the cell behavior *in vitro* and eventually cell-driven osteointegration of implantable devices and *in vivo*.

5. Conclusion

The addition of a block copolymer to a precursor solution of zirconium salt enabled a simple deposition of mesostructured coatings of pure and Ca-doped zirconia. The resulting surfaces were characterized to assess a possible correlation between physicochemical properties and biological activity. The formation of a porous structure (pore size around 5-10 nm) and the addition of calcium as a dopant, induced modification in surface morphology, chemical composition, and wettability. Wettability was found to decrease with Ca content, and to increase with thermal treatment temperature, with the exception of the non porous zirconia treated at 600 °C, that showed increased hydrophobicity. The reasons of such behaviour, perhaps dependent from dehydroxylation, need to be confirmed by further studies. The presence of calcium dopant was found to improve the stability of the mesoporous structure, even at high calcination temperature, perhaps limiting the phase transition mechanisms.

Although further investigations are needed to confirm the hypothesis, a slight increase of the *in vitro* cell viability was noticed for Ca-doped samples. This result, even with a low statistical significance, may be related to the modification in surface patterning and chemistry. Of note, the chemical composition of the starting solution can be easily modified to impart further functionalities to the substrate.

In conclusion, within the limit of this study, we believe that the self-assembly of the mesoporous structures from wet-deposition could be used as a versatile and costless strategy to modify the surface of metal alloys and zirconia dental restoration components, improving the biocompatibility and osseointegration of implantable devices in a next future.

Acknowledgements

This research was supported by Regione Lombardia, Italy, through 'Hot&Cold' project, POR FESR 2014-2020.

References

[1] C.T. Kresge, M.E. Leonowicz, W.J. Roth, J.C. Vartuli, J.S. Beck, Ordered mesoporous molecular sieves synthesized by a liquid-crystal template mechanism, Nature 359 (1992) 710-712.

[2] J.Y. Ying, C.P. Mehnert, M.S. Wong, Synthesis and applications of supramolecular-templated mesoporous materials, Angew. Chem. Int. Ed. 38 (1999) 56-77.

[3] S.W. Boettcher, J. Fan, C.-K. Tsung, Q. Shi, G.D. Stucky, Harnessing the sol-gel process for the assembly of non-silicate mesostructured oxide materials, Acc. Chem. Res. 40 (2007) 784-792.

[4] C. Yu, J. Zhuang, L. Dong, K. Cheng, W. Weng, Effect of hierarchical pore structure on ALP expression of MC3T3-E1 cells on bioglass films, Colloids Surf. B Biointerfaces 156 (2017) 213-220.

[5] V.L. Chavez, L. Song, S. Barua, X. Li, Q. Wu, D. Zhao, K. Rege, B.D. Vogt, Impact of nanopore morphology on cell viability on mesoporous polymer and carbon surfaces, Acta Biomater. 6 (2010) 3035-3043.

[6] F. Gentile, R. La Rocca, G. Marinaro, A. Nicastri, A. Toma, F. Paonessa, G. Cojoc, C. Liberale, F. Benfenati, E. Di Fabrizio, Differential cell adhesion on mesoporous silicon substrates, ACS Appl. Mater. Interfaces 4 (2012) 2903-2911.

[7] A. Srivastav, An overview of metallic biomaterials for bone support and replacement, Biomed. Eng. Trends Mater. Sci. IntechOpen (2011).

[8] A. Siddiqi, A.G.T. Payne, R.K. De Silva, W.J. Duncan, Titanium allergy: could it affect dental implant integration? Clin. Oral Implants Res. 22 (2011) 673-680.

[9] R.C. Garvie, The Cubic Field in the System CaO-ZrO2, J. Am. Ceram. Soc. 51 (1968) 553-556.

[10] M. Filal, C. Petot, M. Mokchah, C. Chateau, J.L. Carpentier, Ionic conductivity of yttrium-doped zirconia and the "composite effect, Solid State Ion. 80 (1995) 27-35.

[11] C.B. Abi, O.F. Emrullahog, G. Said, Microstructure and mechanical properties of MgO-stabilized ZrO2-Al2O3 dental composites, J. Mech. Behav. Biomed. Mater. 18 (2013) 123-131.

[12] S. Wang, J. Li, Z. Zhou, S. Zhou, Z. Hu, Micro-/nano-scales direct cell behavior on biomaterial surfaces, Molecules 24 (2018) 75.

[13] M. Ermis, E. Antmen, V. Hasirci, Micro and Nanofabrication methods to control cell-substrate interactions and cell behavior: a review from the tissue engineering perspective, Bioact. Mater. 3 (2018) 355-369.

[14] G.K. Thakral, R. Thakral, N. Sharma, J. Seth, P. Vashisht, Nanosurface-the future of implants, J. Clin. Diagn. Res. 8 (2014) ZE07.

[15] F. Variola, F. Vetrone, L. Richert, P. Jedrzejowski, J. Yi, S. Zalzal, S. Clair, A. Sarkissian, D.F. Perepichka, J.D. Wuest, Improving biocompatibility of implantable metals by nanoscale modification of surfaces: an overview of strategies, fabrication methods, and challenges, Small 5 (2009) 996-1006.

[16] C. Wirth, B. Grosgogeat, C. Lagneau, N. Jaffrezic-Renault, L. Ponsonnet, Biomaterial surface properties modulate in vitro rat calvaria osteoblasts response: roughness and or chemistry? Mater. Sci. Eng. C 28 (2008) 990-1001.

[17] C.-H. Ku, D.P. Pioletti, M. Browne, P.J. Gregson, Effect of different Ti-6Al-4V surface treatments on osteoblasts behaviour, Biomaterials 23 (2002) 1447-1454.

[18] A. Afzal, Implantable zirconia bioceramics for bone repair and replacement: a chronological review, Mater. Express. 4 (2014) 1-12.

[19] R.A. Delgado-Ruíz, G. Gomez Moreno, A. Aguilar-Salvatierra, A. Markovic, J.E. Mate-Sánchez, J.L. Calvo-Guirado, Human fetal osteoblast behavior on zirconia dental implants and zirconia disks with microstructured surfaces. An experimental in vitro study, Clin. Oral Implants Res. 27 (2016).

[20] M. Araújo, M. Miola, A. Venturello, G. Baldi, J. Pérez, E. Verné, Glass coatings on zirconia with enhanced bioactivity, J. Eur. Ceram. Soc. 36 (2016) 3201-3210.

[21] J.-Z. Yang, R. Sultana, P. Ichim, X.-Z. Hu, Z.-H. Huang, W. Yi, B. Jiang, Y. Xu, Microporous calcium phosphate coatings on load-bearing zirconia substrate: processing, property and application, Ceram. Int. 39 (2013) 6533-6542.

[22] J.L. Calvo-Guirado, A. Aguilar Salvatierra, J. Gargallo-Albiol, R.A. Delgado-Ruiz, J.E. Maté Sanchez, M. Satorres-Nieto, Zirconia with laser-modified microgrooved surface vs. titanium implants covered with melatonin stimulates bone formation. Experimental study in tibia rabbits, Clin. Oral Implants Res. 26 (2015) 1421-1429.

[23] Y. Xu, D. Gao, P. Feng, C. Gao, S. Peng, H. Ma, S. Yang, C. Shuai, A mesoporous silica composite scaffold: cell behaviors, biomineralization and mechanical properties, Appl. Surf. Sci. 423 (2017) 314-321.

[24] J.-P. St-Pierre, M. Gauthier, L.-P. Lefebvre, M. Tabrizian, Three-dimensional growth of differentiating MC3T3-E1 pre-osteoblasts on porous titanium scaffolds, Biomaterials 26 (2005) 7319-7328.

[25] Z. Sun, Y. Deng, J. Wei, D. Gu, B. Tu, D. Zhao, Hierarchically ordered macro-/mesoporous silica monolith: tuning macropore entrance size for size-selective adsorption of proteins, Chem. Mater. 23 (2011) 2176-2184.

[26] Y. Ma, P. Rajendran, C. Blum, Y. Cesa, N. Gartmann, D. Brühwiler, V. Subramaniam, Microspectroscopic analysis of green fluorescent proteins infiltrated into mesoporous silica nanochannels, J. Colloid Interface Sci. 356 (2011) 123-130.

[27] Z. Özkurt, E. Kazazoğlu, Zirconia dental implants: a literature review, J. Oral Implantol. 37 (2011) 367-376.

[28] G.J. de AA Soler-Illia, E.L. Crepaldi, D. Grosso, C. Sanchez, Block copolymer-templated mesoporous oxides, Curr. Opin. Colloid Interface Sci. 8 (2003) 109-126.
[29] F. Kleitz, S.J. Thomson, Z. Liu, O. Terasaki, F. Schüth, Porous mesostructured zirconium oxophosphate with cubic (Ia 3 d) symmetry, Chem. Mater. 14 (2002) 4134-4144.
[30] E.L. Crepaldi, S. de AA, J. Galo, A. Bouchara, D. Grosso, D. Durand, C. Sanchez, Controlled formation of highly ordered cubic and hexagonal mesoporous nanocrystalline yttria-zirconia and ceria-zirconia thin films exhibiting high thermal stability, Angew. Chem. Int. Ed. 42 (2003) 347-351.
[31] A.E. Danks, S.R. Hall, Z. Schnepp, The evolution of "sol-gel"chemistry as a technique for materials synthesis, Mater. Horizons 3 (2016) 91-112.
[32] G.J.A.A. Soler-Illia, O. Azzaroni, Multifunctional hybrids by combining ordered mesoporous materials and macromolecular building blocks, Chem. Soc. Rev. 40 (2011) 1107-1150.
[33] C.J. Brinker, D.R. Dunphy, Morphological control of surfactant-templated metal oxide films, Curr. Opin. Colloid Interface Sci. 11 (2006) 126-132.
[34] B. Feng, J. Chen, X. Zhang, Interaction of calcium and phosphate in apatite coating on titanium with serum albumin, Biomaterials 23 (2002) 2499-2507.
[35] N.Y. Hou, J. Zhu, H. Zhang, H. Perinpanayagam, Ultrafine calcium-titania-polyester dry powder coatings promote human mesenchymal cell attachment and biomineralization, Surf. Coat. Technol. 251 (2014) 177-185.
[36] S. Nath, N. Sinha, B. Basu, Microstructure, mechanical and tribological properties of microwave sintered calcia-doped zirconia for biomedical applications, Ceram. Int. 34 (2008) 1509-1520.
[37] Q. Yuan, L.-L. Li, S.-L. Lu, H.-H. Duan, Z.-X. Li, Y.-X. Zhu, C.-H. Yan, Facile synthesis of Zr-based functional materials with highly ordered mesoporous structures, J. Phys. Chem. C 113 (2009) 4117-4124.
[38] M.J. Dalby, N. Gadegaard, R. Tare, A. Andar, M.O. Riehle, P. Herzyk, C.D.W. Wilkinson, R.O.C. Oreffo, The control of human mesenchymal cell differentiation using nanoscale symmetry and disorder, Nat. Mater. 6 (2007) 997.
[39] B.L. Kirsch, E.K. Richman, A.E. Riley, S.H. Tolbert, In-situ X-ray diffraction study of the crystallization kinetics of mesoporous titania films, J. Phys. Chem. B 108 (2004) 12698-12706.
[40] J. Chen, Z. Cai, X. Chen, X. Zheng, Y. Zheng, Facile synthesis of ordered mesoporous CaO-ZrO 2 composite with mild conditions, Mater. Lett. 168 (2016) 214-217.
[41] R.C. Garvie, Stabilization of the tetragonal structure in zirconia microcrystals, J. Phys. Chem. 82 (1978) 218-224.
[42] A. Mikó, A.L. Demirel, M. Somer, Synthesis and characterization of mesoporous zirconium oxide thin films, IOP Conf. Ser. Mater. Sci. Eng, IOP Publishing, 2010 p. 12019.
[43] S. Fabris, A.T. Paxton, M.W. Finnis, A stabilization mechanism of zirconia based on oxygen vacancies only, Acta Mater. 50 (2002) 5171-5178.
[44] X. Tian, T. Xiao, C. Yang, Z. Zhou, H. Ke, Synthesis of crystalline ordered mesoporous CaO-ZrO 2 solid solution as a promising solid base, Mater. Chem. Phys. 124 (2010) 744-747.
[45] Q. Yu, W. Fu, C. Yu, H. Yang, R. Wei, Y. Sui, S. Liu, Z. Liu, M. Li, G. Wang, Structural, electrical and optical properties of yttrium-doped ZnO thin films prepared by sol-gel method, J. Phys. D Appl. Phys. 40 (2007) 5592.
[46] F. Rupp, R.A. Gittens, L. Scheideler, A. Marmur, B.D. Boyan, Z. Schwartz, J. Geis-Gerstorfer, A review on the wettability of dental implant surfaces I: theoretical and experimental aspects, Acta Biomater. 10 (2014) 2894-2906.
[47] F. Namavar, C.L. Cheung, R.F. Sabirianov, W.-N. Mei, X.C. Zeng, G. Wang, H. Haider, K.L. Garvin, Lotus effect in engineered zirconia, Nano Lett. 8 (2008) 988-996.